INTERNATIONAL JOURNAL FOR NUMERICAL AND ANALYTICAL METHODS IN GEOMECHANICS
Int. J. Numer. Anal. Meth. Geomech. 2009; **33**:1889–1905
Published online 1 June 2009 in Wiley InterScience (www.interscience.wiley.com). DOI: 10.1002/nag.810

Observations on the extended Matsuoka–Nakai failure criterion

D. V. Griffiths*,† and Jinsong Huang

Division of Engineering, Colorado School of Mines, Golden, CO 80401, U.S.A.

SUMMARY

The equivalent Mohr–Coulomb (M-C) friction angle ϕ'_{mc} (*J. Geotech. Eng.* 1990; **116**(6):986–999) of the extended Matsuoka–Nakai (E-M-N) criterion has been examined under all possible stress paths. It is shown that ϕ'_{mc} depends only on the ratio of cohesion to confining stress c'/σ'_3 and the frictional angle ϕ'_c, where ϕ'_c is the friction angle measured in triaxial compression (or extension) to which the E-M-N surface is fitted. It is also shown that ϕ'_{mc} is independent of c', when $\sigma'_3=0$ and of σ'_3 when $c'=0$, with the former representing an upper bound and the latter a lower bound of ϕ'_{mc} for any particular stress path. The closest point projection method has also been implemented successfully with the E-M-N criterion, and plane strain and axisymmetric element tests performed to verify some theoretical predictions relating to failure and post-yielding behavior. Finally, a bearing capacity problem was analyzed using both E-M-N and M-C, highlighting the conservative nature of M-C for different friction angles. Copyright © 2009 John Wiley & Sons, Ltd.

Received 18 September 2008; Revised 17 December 2008; Accepted 31 March 2009

KEY WORDS: failure criterion; Matsuoka–Nakai; Mohr–Coulomb; finite element method; closest point projection method; elastoplasticity

1. INTRODUCTION

Prediction of failure stresses for frictional/cohesive soils has traditionally been based on the Mohr–Coulomb (M-C) criterion, which can be written in the form $f=0$, where

$$f=\tfrac{1}{2}(\sigma'_1+\sigma'_3)\sin\phi'_c-\tfrac{1}{2}(\sigma'_1-\sigma'_3)-c'\cos\phi'_c \tag{1}$$

where c' and ϕ'_c are the cohesion and friction angle, and σ'_1 and σ'_3 are the major and minor principal effective stresses. A tension-positive sign convention is assumed throughout.

*Correspondence to: D. V. Griffiths, Division of Engineering, Colorado School of Mines, Golden, CO 80401, U.S.A.
†E-mail: d.v.griffiths@mines.edu

Contract/grant sponsor: NSF; contract/grant number: CMS-0408150

The M-C criterion has been criticized on the grounds that it takes no account of the intermediate principal stress σ'_2. Based on the spatially mobilized plane concept, Matsuoka and Nakai (M-N) [1] proposed a criterion for cohesionless soil

$$\frac{(\sigma'_1\sigma'_2+\sigma'_2\sigma'_3+\sigma'_3\sigma'_1)(\sigma'_1+\sigma'_2+\sigma'_3)}{\sigma'_1\sigma'_2\sigma'_3}=K_{\mathrm{MN}} \tag{2}$$

where the material constant K_{MN} has been shown (e.g. [2]) to be given by

$$K_{\mathrm{MN}}=\frac{9-\sin^2\phi'_c}{1-\sin^2\phi'_c} \tag{3}$$

In order to extend the M-N criterion to that for frictional and cohesive material, the normal stress can be shifted as

$$\hat{\sigma}=\sigma'+\sigma_0 \tag{4}$$

where $\sigma_0=-c'\cot\phi'_c$.

When the M-N criterion has been shifted in this way, it is then called the extended Matsuoka–Nakai (E-M-N) criterion (e.g. [3–5]). The E-M-N criterion reduces to the von-Mises criterion when $\sigma_0\to\infty$ or when $\phi'_c=0.0$ for $c'\neq 0$.

As shown in Figure 1, E-M-N coincides with M-C at all apexes corresponding to triaxial extension and compression.

Griffiths [2, 6] examined the M-N criterion in relation to the M-C criterion and proposed the concept of an equivalent friction angle ϕ'_{mc} as the angle of friction of the equivalent M-C surface that would pass through a particular point in stress space under consideration. This approach enables direct comparisons to be made between different failure criteria using a familiar soil mechanics parameter. In the same paper a method involving the solution of a cubic equation was presented for determining ϕ'_{mc} for the M-N failure surface. This concept is adopted in this current paper to further investigate the E-M-N criterion.

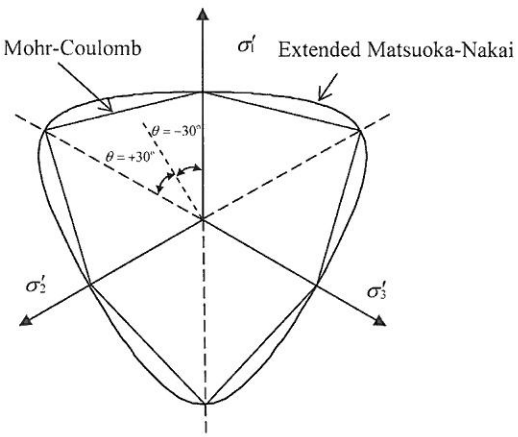

Figure 1. Mohr–Coulomb and extended Matsuoka–Nakai criteria.

DOI: 10.1002/nag

Furthermore, while examining conical 'Drucker–Prager' failure criteria it was shown that following first yield, the angular stress invariant changes during a post-yielding phase until maximum dilatancy $\psi_{\max}$ is achieved, where ψ is a dilation angle, which has an analogous relationship to the plastic potential surface that ϕ'_{mc} has to the failure surface. A similar phenomenon with the E-M-N criterion is tested in this paper.

Borja *et al.* [7] applied the closest point projection method (CPPM) (e.g. [8, 9]) in principal stress space to the M-N criterion, and Matsuoka and Sun [5] presented the general stress–strain relations for the E-M-N criterion. To the authors knowledge, however, no work has been reported involving implicit integration of the E-M-N criterion.

In this paper, the CPPM method is successfully applied to the E-M-N criterion and used to model plane strain and axisymmetric element tests to verify some theoretical predictions relating to failure and post-yielding behavior. Finally, a bearing capacity problem is analyzed using both E-M-N and M-C, highlighting the conservative nature of M-C for different friction angles.

2. EQUIVALENT M-C FRICTION ANGLE OF E-M-N

We start with a brief review of the stress invariants needed to navigate principal stress space.

A stress point in principal stress space can be defined using the invariants (see, e.g. Smith and Griffiths [10])

$$(s, t, \theta) \tag{5}$$

where

$$s = \frac{1}{\sqrt{3}}(\sigma'_x + \sigma'_y + \sigma'_z) \tag{6}$$

$$t = \frac{1}{\sqrt{3}}[(\sigma'_x - \sigma'_y)^2 + (\sigma'_y - \sigma'_z)^2 + (\sigma'_z - \sigma'_x)^2 + 6\tau_{xy}^2 + 6\tau_{yz}^2 + 6\tau_{zx}^2]^{1/2} \tag{7}$$

and

$$\theta = \frac{1}{3}\arcsin\left(\frac{-3\sqrt{6}J_3}{t^3}\right) \tag{8}$$

which is also known as the Lode angle.

The third deviatoric stress invariant is given as

$$J_3 = s_x s_y s_z - s_x\tau_{yz}^2 - s_y\tau_{zx}^2 - s_z\tau_{xy}^2 + 2\tau_{xy}\tau_{yz}\tau_{zx} \tag{9}$$

where $s_x = (2\sigma'_x - \sigma'_y - \sigma'_z)/3$, etc.

In this notation, s gives the perpendicular distance of the π-plane from the origin, and (t, θ) act as polar coordinates within that plane. The invariants given in Equations (6) and (7) are convenient because they represent actual lengths in principal stress space. Equation (2) can be expressed in (s, t, θ) space as

$$f = -\sqrt{2}K_{\mathrm{MN}}\sin(3\theta)t^3 + (9 - 3K_{\mathrm{MN}})t^2 s + (2K_{\mathrm{MN}} - 18)s^3 = 0 \tag{10}$$

DOI: 10.1002/nag

Principal stresses are easily obtained from these invariants as

$$\begin{aligned}\sigma'_1 &= \frac{s}{\sqrt{3}} + \sqrt{\frac{2}{3}} t \sin\left(\theta - \frac{2\pi}{3}\right)\\ \sigma'_2 &= \frac{s}{\sqrt{3}} + \sqrt{\frac{2}{3}} t \sin\theta\\ \sigma'_3 &= \frac{s}{\sqrt{3}} + \sqrt{\frac{2}{3}} t \sin\left(\theta + \frac{2\pi}{3}\right)\end{aligned} \tag{11}$$

The angular invariant θ from (8) is constrained to vary in the range $-30° \leqslant \theta \leqslant 30°$. Note that since $\sin(\theta+2\pi/3) \geqslant \sin\theta \geqslant \sin(\theta-2\pi/3)$, Equation (11) ensures that σ'_1 is the smallest of the three principal stresses and hence the most compressive.

Bishop [11] defined a more intuitive parameter b, which gives the magnitude of σ'_2 relative to σ'_1 and σ'_3, where

$$b = (\sigma'_2 - \sigma'_3)/(\sigma'_1 - \sigma'_3) \tag{12}$$

It is easily shown that the angular invariant is related to Bishop's b as follows:

$$\theta = \arctan((1-2b)/\sqrt{3}) \tag{13}$$

As the angular invariant θ from (8) varies in the range $-30° \leqslant \theta \leqslant 30°$, b varies in the range $1 \geqslant b \geqslant 0$. The lower bound $\theta = -30°$ (or $b = 1.0$) corresponds to a positive principal axis in the π-plane and triaxial extension conditions, whereas the upper bound $\theta = 30°$ (or $b = 0.0$) corresponds to a negative principal axis in the π-plane and triaxial compression conditions. All other stress conditions correspond to the intermediate values of θ. For example, plane strain corresponds to a positive θ and $0.5 \geqslant b \geqslant 0$, where in elastic case, parameter b equals Poisson's ratio.

The present work will show that for a given stress path (θ=constant) ϕ'_{mc} reaches a lower bound for cohesionless soils ($\sigma'_3 > 0$, $c' = 0$) and an upper bound for unconfined compression of cohesive soils ($\sigma'_3 = 0$, $c' > 0$).

The E-M-N can be obtained by modifying the M-N criterion from Equation (2) to give

$$\frac{[(\sigma'_1+\sigma_0)(\sigma'_2+\sigma_0)+(\sigma'_2+\sigma_0)(\sigma'_3+\sigma_0)+(\sigma'_1+\sigma_0)(\sigma'_3+\sigma_0)](\sigma'_1+\sigma'_2+\sigma'_3+3\sigma_0)}{(\sigma'_1+\sigma_0)(\sigma'_2+\sigma_0)(\sigma'_3+\sigma_0)} = K_{MN} \tag{14}$$

where $\sigma_0 = -c' \cot\phi'_{mc}$.

For a given constant b stress path, $\sigma'_2 = b\sigma'_1 + (1-b)\sigma'_3$ and

$$\frac{\left[\left(\frac{\sigma'_1}{\sigma'_3} - \frac{c'\cot\phi'_c}{\sigma'_3}\right)\left(\frac{b\sigma'_1}{\sigma'_3} + 1 - b - \frac{c'\cot\phi'_c}{\sigma'_3}\right) + \left(\frac{b\sigma'_1}{\sigma'_3} + 1 - b - \frac{c'\cot\phi'_c}{\sigma'_3}\right)\left(1 - \frac{c'\cot\phi'_c}{\sigma'_3}\right) + \left(\frac{\sigma'_1}{\sigma'_3} - \frac{c'\cot\phi'_c}{\sigma'_3}\right)\left(1 - \frac{c'\cot\phi'_c}{\sigma'_3}\right)\right]\left(\frac{\sigma'_1}{\sigma'_3} + \frac{b\sigma'_1}{\sigma'_3} + 2 - b - \frac{3c'\cot\phi'_c}{\sigma'_3}\right)}{\left(\frac{\sigma'_1}{\sigma'_3} - \frac{c'\cot\phi'_c}{\sigma'_3}\right)\left(\frac{b\sigma'_1}{\sigma'_3} + 1 - b - \frac{c'\cot\phi'_c}{\sigma'_3}\right)\left(1 - \frac{c'\cot\phi'_c}{\sigma'_3}\right)}$$

$$= K_{mn} \tag{15}$$

while M-C

$$\frac{\sigma'_1}{\sigma'_3} = K_p + \frac{2c'}{\sigma'_3}\sqrt{K_p} \tag{16}$$

where $K_p = \tan^2(45 + \phi'_{mc}/2)$.

DOI: 10.1002/nag

Substituting Equation (16)–(15), it can be seen that the equivalent friction angle ϕ'_{mc} depends only on ϕ'_c, b and c'/σ'_3.

For the special case of $\sigma'_3=0$, E-M-N from Equation (15) becomes

$$\frac{\left[-\cot\phi'_c\left(b\frac{\sigma'_1}{c'}-\cot\phi'_c\right)+\left(b\frac{\sigma'_1}{c'}-\cot\phi'_c\right)\left(\frac{\sigma'_1}{c'}-\cot\phi'_c\right)-\cot\phi'_c\left(\frac{\sigma'_1}{c'}-\cot\phi'_c\right)\right]\left(b\frac{\sigma'_1}{c'}+\frac{\sigma'_1}{c'}-3\cot\phi'_c\right)}{-\cot\phi'_c\left(b\frac{\sigma'_1}{c'}-\cot\phi'_c\right)\left(\frac{\sigma'_1}{c'}-\cot\phi'_c\right)}=K_{MN} \tag{17}$$

while M-C can be written as

$$\frac{\sigma'_1}{c'}=2\sqrt{K_p} \tag{18}$$

Substituting Equation (18)–(17), it can be seen that the equivalent friction angle ϕ'_{mc} depends only on ϕ'_c and b.

If $c'=0$, the E-M-N reduces to M-N and can be expressed as

$$\frac{\left[\frac{\sigma'_1}{\sigma'_3}\left(b\frac{\sigma'_1}{\sigma'_3}+1-b\right)+(1+b)\frac{\sigma'_1}{\sigma'_3}+1-b\right]\left[(1+b)\frac{\sigma'_1}{\sigma'_3}+2-b\right]}{d\frac{\sigma'_1}{\sigma'_3}\left(b\frac{\sigma'_1}{\sigma'_3}+1-b\right)}=K_{MN} \tag{19}$$

For M-C, if $c'=0$:

$$\frac{\sigma'_1}{\sigma'_3}=K_p \tag{20}$$

Substituting Equation (20) into (19), it can be seen that ϕ'_{mc} only dependent on ϕ'_c and b.

The general procedure to determine ϕ'_{mc} is summarized here:

(1) Given σ'_3, c' and ϕ'_c.
(2) For a particular stress path defined by $0\leqslant b\leqslant 1$, compute

$$\sigma'_2=b\sigma'_1+(1-b)\sigma'_3 \tag{21}$$

(3) Solve Equation (15) for σ'_1.
(4) Back figure ϕ'_{mc} using

$$\phi'_{mc}=-\frac{1}{2}\pi+2\arctan\left(\frac{-c'+\sqrt{c'^2+\sigma'_1\sigma'_3}}{\sigma'_3}\right) \tag{22}$$

For the particular case of $\phi'_c=30°$, ϕ'_{mc} has been found using this procedure for a range of stress paths as shown in Figure 2. For all stress paths it can be seen that the ϕ'_{mc} increases as c'/σ_3 increases. The value of ϕ'_{mc} reaches an upper bound when $\sigma'_3=0(c'/\sigma_3=\infty)$ and a lower bound when $c'=0(c'/\sigma_3=0)$. The upper and lower bounds of ϕ'_{mc} for $\phi'_c=10°$, $20°$, $30°$ and $40°$ are plotted in Figure 3.

DOI: 10.1002/nag

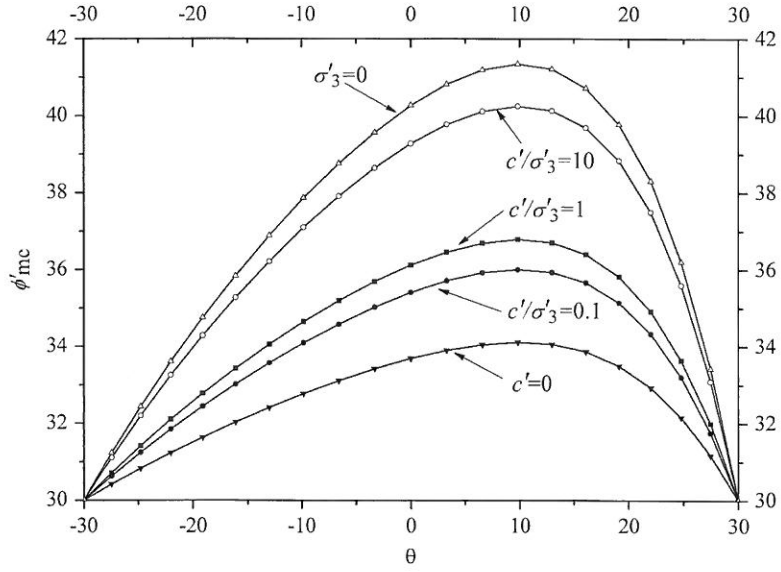

Figure 2. ϕ'_{mc} verses θ for different values of c'/σ'_3 when $\phi'_c = 30°$.

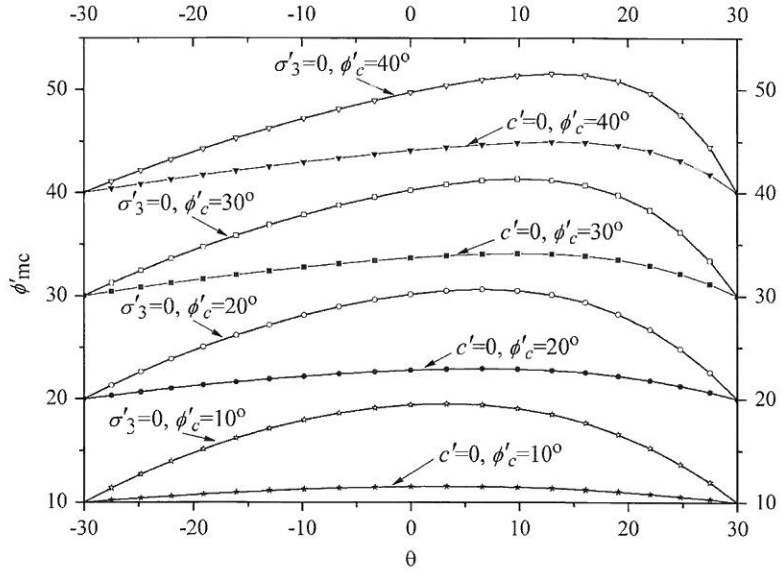

Figure 3. Upper and lower bounds of ϕ'_{mc}.

3. STRESS RATIO AT FAILURE

The stress ratio $R_f = \sigma'_1/\sigma'_3$ ($R_f = K_p$ for M-C when $c' = 0$ for a soil at failure) is a convenient measure of cohesionless soil strength, and it is of interest to note the values of R_f predicted by M-N criterion.

DOI: 10.1002/nag

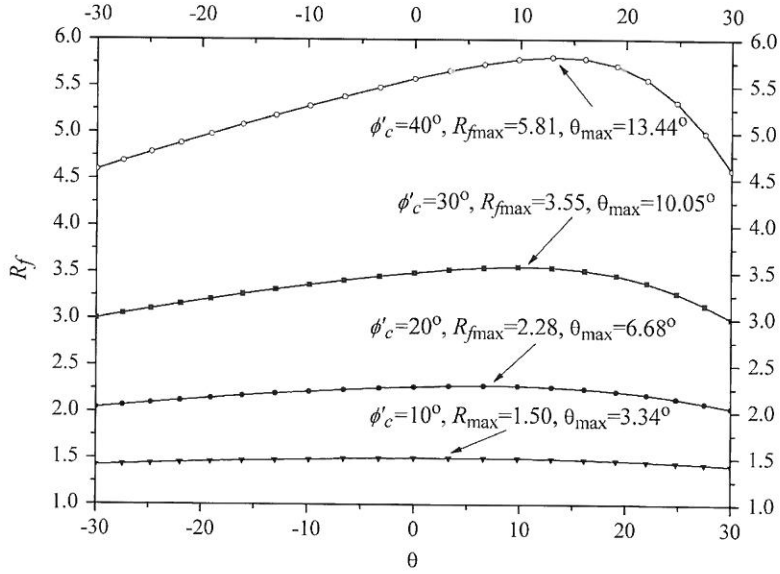

Figure 4. R_f predicted by the M-N criterion for different stress paths.

It can be seen from Equation (19) that R_f depends only on ϕ'_c and b. Equation (19) can be rearranged as

$$(b+b^2)R_f^3+(2+4b-K_{MN}b-b^2)R_f^2+(K_{MN}b-b^2-2b+5)R_f+b^2-3b+2=0 \tag{23}$$

For a given stress path and ϕ'_c, R_f can be easily obtained by solving Equation (23).

To decide the maximum R_f values and the corresponding Lode angles at which the maximum occurs, take the partial derivative of Equation (23) with respect to b and let $\partial R_f/\partial b=0$ to give

$$(1+2b)R_f^3+(4-K_{MN}-2b)R_f^2+(K_{MN}-2b-2)R_f+2b-3=0 \tag{24}$$

Solving Equations (23) and (24) and select the positive real root

$$b_{\max}=\frac{1}{2}-\frac{1}{2}\sqrt{\frac{\sqrt{K_{MN}}-3}{\sqrt{K_{MN}}+1}} \tag{25}$$

$$R_{f\max}=-\frac{1}{2}+\frac{1}{2}K_{MN}-\sqrt{K_{MN}}+\frac{1}{2}\sqrt{(\sqrt{K_{MN}}-3)(\sqrt{K_{MN}}-1)(K_{MN}-1)} \tag{26}$$

The results of R_f for $\phi'_c=10°$, 20°, 30° and 40° are plotted in Figure 4. Also highlighted in Figure 4 are $R_{f\max}$ values and the corresponding Lode angles at which the maximum occurred.

4. SINGLE ELEMENT TEST

An important method for the implementation of failure criteria in boundary-value problems modeled using the finite element method is the CPPM (e.g. [8, 9]). The iteration procedure shown in

DOI: 10.1002/nag

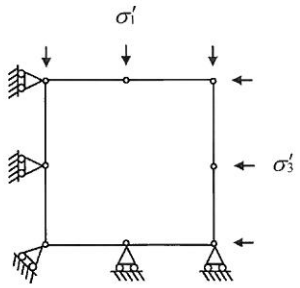

Figure 5. Single element test.

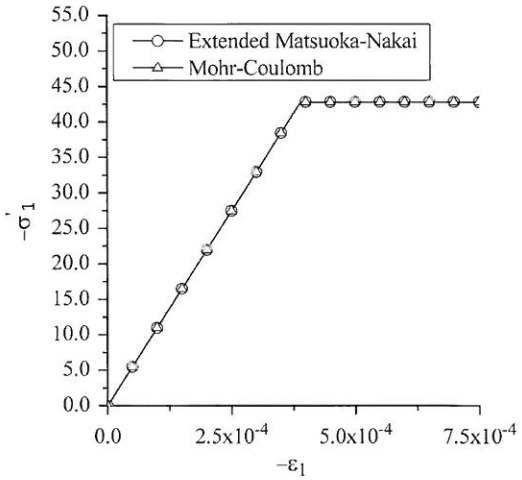

Figure 6. Results of axisymmetric single element test.

Appendix A was implemented within the program structure described in the text by Smith and Griffiths [10]. The authors initially tried returning the stress in general stress space but encountered numerical convergence difficulties. The explanation for the difficulties lies in the observation that the M-N criterion is highly curved (e.g. [12, 13]). The algorithm used by the authors returned the stresses in principal stress space using similar tensor operations as described by Larsson and Runesson [14]. For the interested reader, the required derivatives are given in Appendix B. The consistent elastoplastic modulus (e.g. [14]) is given in Appendix C.

A single 8-node plane strain element was loaded as shown in Figure 5. Displacement control was used with an increment of 10^{-7} m. A non-associated flow rule was assumed ($\psi=0$). Young's Modulus was fixed at $E=10^5\,\mathrm{kN/m^2}$.

4.1. Axisymmetric c'–ϕ' soil

The first validation example was of an initially unconfined ($\sigma'_1=\sigma'_2=\sigma'_3=0$) axisymmetric element of soil with $c'=15\,\mathrm{kN/m^2}$ and $\phi'_c=20°$ and Poisson's ratio $\upsilon=0.3$. The axial stress σ'_1 was then gradually increased to failure.

DOI: 10.1002/nag

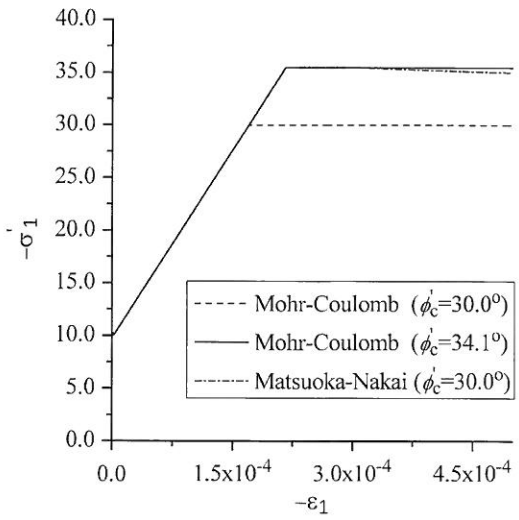

Figure 7. Plane strain single element test for friction soil.

The theoretical failure load according to both M-C (Equation (1)) and E-M-N (Equations (2) and (3)) is $\sigma'_{1f} = -42.84\,\mathrm{kN/m^2}$, and the numerical results were in essentially exact agreement as shown in Figure 6.

4.2. *Plane strain cohesionless (ϕ', $c'=0$) soil*

The second validation example was of a plane strain element of soil with $c'=0$ and $\phi'_c=30°$, initially confined isotropically to $\sigma'_1=\sigma'_2=\sigma'_3=-10\,\mathrm{kN/m^2}$. Poisson's ratio was set to 0.4 (corresponding $\theta=6.6°$ from Equation (13)), which from the procedure described previously will lead at first yield to $\phi'_{\mathrm{mc}}=34.1°$. The axial stress at failure stress by M-C (Equation (1)) is $\sigma'_{1f}=-30.0\,\mathrm{kN/m^2}$, whereas by the M-N criterion (Equations (2) and (3)) it is $\sigma'_{1f}=-35.45\,\mathrm{kN/m^2}$. The finite element results for this example are in close agreement with the analytical results as shown in Figure 7. It can be seen that the M-N criterion gave 18% higher compressive strength than M-C in this case. It should be mentioned that the results obtained by M-N criterion show small numerical drifting.

4.3. *Plane strain c'–ϕ' soil*

The third validation example was once more a plane strain element of soil, but this time with both cohesion and friction given by $c'=15.0\,\mathrm{kN/m^2}$ and $\phi'_c=20°$. The sample was initially unconfined ($\sigma'_1=\sigma'_2=\sigma'_3=0$) before the application of axial loading. Poisson's ratio was set to 0.3, which from Equation (13) leads to an elastic stress path defined by $\theta=13°$. From the general procedure described earlier this stress path leads to first yield at $\phi'_{\mathrm{mc}}=31.0°$.

Note that the parameters in this example are the same as in the axisymmetric case considered previously, hence the M-C criterion predicts the same failure load since σ'_2 is ignored. In this case, however, the E-M-N criterion gives $\sigma'_{1f}=-52.07\,\mathrm{kN/m^2}$ which is 22% higher. The M-C criterion

DOI: 10.1002/nag

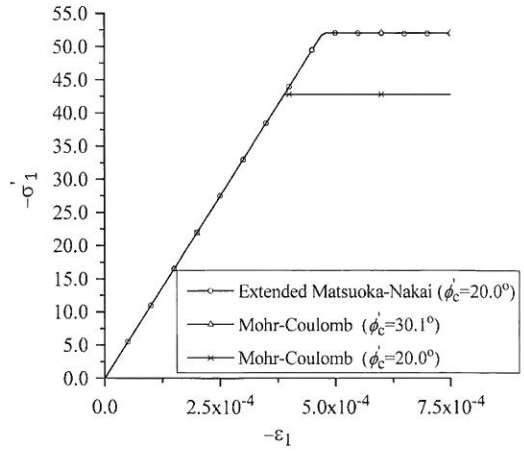

Figure 8. Plane strain single element test for c'–ϕ' soil.

as shown in Figure 8 would require a friction angle some 10.1° higher (>50%) than E-M-N to give the same strength.

5. ELASTOPLASTIC BEHAVIOR UNDER PLANE STRAIN CONDITIONS

In studies of conical 'Drucker–Prager' failure criteria (e.g. [2]) it was shown that following first yield, the angular stress invariant changed or 'drifted' during a post-yielding phase until maximum dilatancy ψ_{max} was achieved. This phenomenon is tested in this section by considering a plane strain finite element test implementing M-N with $\psi > 0$.

Consider a single element plane strain test with $c'=0.0$, $\phi_c'=\psi=40°$, $E=10^5\,\mathrm{kN/m^2}$ and $\upsilon=0.05$ subjected to an initial isotropic stress of $\sigma_1'=\sigma_2'=\sigma_3'=-10.0\,\mathrm{kN/m^2}$ prior to increasing the axial stress to failure. From Equation (13), the Lode angle is given by $\theta=27.46°$, which corresponds to $\phi_{mc}'=41.8°$ (Figure 3) or a stress ratio of $R=5.0$ (Figure 4). With $\psi=40°$, the stresses then drift to the point of maximum dilation that occurs at $\theta=13.44°$ giving by $\phi_{mc}'=44.9°$ (Figure 3) or $R=5.81$ (Figure 4). The results of the single element test shown in Figure 9 confirm these predictions and also give results for non-associated flow rules in which $\psi=0°$ and $\psi=20°$, which have lower ultimate stress ratios than the associated flow rule.

6. NUMERICAL EXAMPLE OF A BOUNDARY-VALUE PROBLEM

A classical footing bearing capacity problem has been analyzed using both E-M-N and M-C. Figure 10 shows a mesh involving 32 elements with a flexible strip footing at the surface of a layer of uniform weightless soil. The footing supports a uniform stress q, which is increased incrementally to failure. The mesh consists of 8-noded quadrilateral elements with 'reduced' (4 Gauss points) integration. The cohesion is fixed at $c'=15\,\mathrm{kN/m^2}$ and several friction angles were

DOI: 10.1002/nag

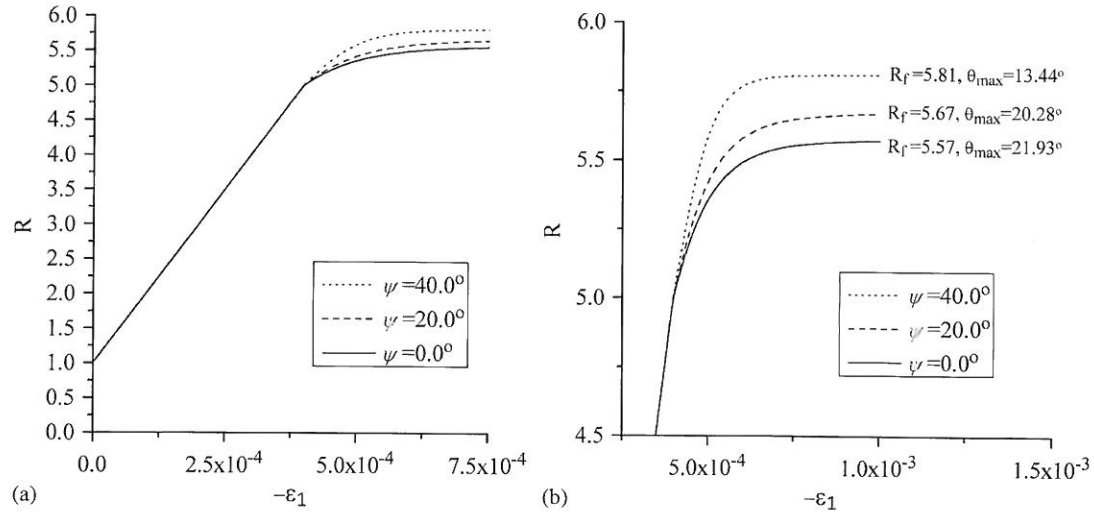

Figure 9. Ultimate stress ratio of M-N when $\phi'_c = 40°$.

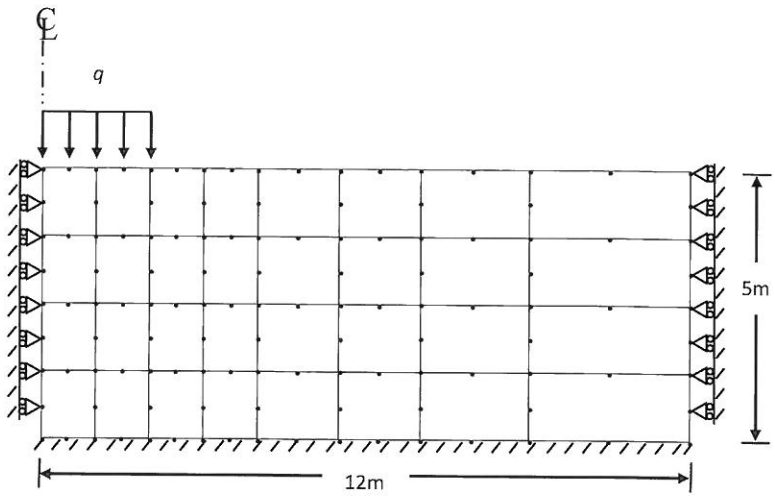

Figure 10. Mesh of a strip footing.

considered in the range $5° \leqslant \phi'_c \leqslant 40°$. The dilation angle ψ was set to zero. The elastic parameters were $E = 1 \times 10^5\,\mathrm{kN/m^2}$ and $\upsilon = 0.3$.

Theoretically, bearing failure in this problem occurs when q reaches the load given by

$$q_{\mathrm{ult}} = cN_c \tag{27}$$

where N_c is the bearing capacity factor for soil cohesion [15]

$$N_c = (N_q - 1)\cot\phi'_c \tag{28}$$

DOI: 10.1002/nag

Table I. Bearing capabilities of a strip footing.

ϕ'_c (deg.)	Prandtl (kN/m^2)	q_{mc} (kN/m^2)	q_{emn} (kN/m^2)	$(q_{emn}-q_{mc})/q_{mc}$ (%)
5	97	99	119	20
10	125	127	159	25
20	223	221	308	39
30	452	452	706	56
40	1130	1102	2268	106

where

$$N_q = \tan^2\left(45+\frac{\phi'_c}{2}\right)e^{\pi\tan\phi'_c} \tag{29}$$

The results of finite element analyses compared with predictions from the Prandtl formula are summarized in Table I, where q_{mc} and q_{emn} are the results of M-C and E-M-N, respectively. It can be seen that the M-C gave close agreement with Prandtl's formula; however, the E-M-N generally predicted much higher bearing values. The difference between the results predicted by M-C and E-M-N increased with the input friction angle to the point where the E-M-N bearing capacity for an input of $\phi'_c=40°$ was more than double the value predicted by M-C.

The higher bearing capacity predicted by E-M-N is to be expected since this criterion predicts higher strength than M-C for all stress paths (except triaxial compression and extension). Since the E-M-N criterion is based on carefully conducted 'true triaxial' laboratory tests that properly account for the influence of σ'_2, it should be considered a more accurate model of soil strength than M-C. The M-C criterion remains popular in geomechanics, however, on account of its simplicity and conservatism, in addition to the fact that it forms the basis of many theoretical results in classical soil mechanics.

7. CONCLUSIONS

The paper has described detailed comparisons between the E-M-N and M-C failure criteria. The equivalent friction angle ϕ'_{mc} predicted by the E-M-N criterion with respects to the M-C criterion was examined theoretically under all possible stress paths. It was shown that the ϕ'_{mc} in the E-M-N criterion depends only on c'/σ'_3 and ϕ'_c for a given stress path. It is also shown that ϕ'_{mc} reaches a lower bound when $c'=0$ and an upper bound when $\sigma'_3=0$. The CPPM was applied successfully to an elastoplastic finite element algorithm implementing the E-M-N failure criterion. Plane strain and axisymmetric single element tests were performed to verify the theoretical predictions including post-yielding behavior of M-N under plane strain conditions. Finally, a bearing capacity problem was analyzed using E-M-N and M-C highlighting their different predictions for different input friction angles. As might be expected, the higher the input friction angle, the greater the differences between M-C and E-M-N however the difference could be quite significant. For the case of $\phi'_c=40°$, which was the highest input friction angle considered in this study, E-M-N predicted a bearing capacity that was more than double the value predicted by M-C and classical bearing capacity formulas.

DOI: 10.1002/nag

APPENDIX A: ITERATION PROCEDURE USED IN THE CPPM

In the CPPM, the increments of plastic strain are calculated at the end of the step and the yield condition is enforced at the end of the step. The integration in elastoplastic solutions is always taken over the full load step in each iteration. The integration scheme is written as

1. *Initialization*: Set initial values of plastic strain to converged values at end of previous load step, zero the incremental plasticity parameter and evaluate the elastic trial stress

$$k=0:\ \boldsymbol{\varepsilon}_{n+1}^{\mathrm{p}(0)}=\boldsymbol{\varepsilon}_{n}^{\mathrm{p}},\quad \Delta\lambda^{(0)}=0,\quad \boldsymbol{\sigma}^{(0)}=\mathbf{D}^{\mathrm{e}}(\boldsymbol{\varepsilon}_{n+1}-\boldsymbol{\varepsilon}^{\mathrm{p}(0)})$$

   where $\mathbf{D}^{\mathrm{e}}$ is the elastic modulus, n is the load step number, $\boldsymbol{\varepsilon}^{\mathrm{p}}$ is the plastic strain
2. *Check yield condition and convergence at kth iteration*:

$$f^{(k)}=f(\boldsymbol{\sigma}^{(k)}),\quad \mathbf{r}^{(k)}$$

   where $\mathbf{r}^{(k)}=-[\mathbf{D}^{\mathrm{e}}]^{-1}\Delta\boldsymbol{\sigma}^{(k)}-\Delta\lambda^{(k)}\Delta\mathbf{q}^{(k)}-\delta\lambda^{(k)}\mathbf{q}^{(k)}$ and

$$\mathbf{q}=\frac{\partial g}{\partial\boldsymbol{\sigma}}$$

$$\Delta\mathbf{q}^{(k)}=\frac{\partial\mathbf{q}^{(k)}}{\partial\boldsymbol{\sigma}}\Delta\boldsymbol{\sigma}^{(k)}$$

   where g is the plastic potential function
   If $F^{(k)}<\mathrm{TOL}_1$ and $\|\mathbf{r}^{(k)}\|<\mathrm{TOL}_2$, converged
   else go to 3.
3. *Compute increment in plasticity parameter*:

$$\mathbf{R}^{(k)}=\left[\mathbf{I}+\Delta\lambda^{(k)}\mathbf{D}^{\mathrm{e}}\left[\frac{\partial\mathbf{q}}{\partial\boldsymbol{\sigma}}^{(k)}\right]\right]^{-1}\mathbf{D}^{\mathrm{e}}$$

$$\delta\lambda^{(k)}=\frac{f^{(k)}-\mathbf{f}^{(k)\mathrm{T}}\mathbf{R}^{(k)}\mathbf{r}^{(k)}}{\mathbf{f}^{(k)\mathrm{T}}\mathbf{R}^{(k)}\mathbf{q}^{(k)}}$$

   where $\mathbf{f}=\partial f/\partial\boldsymbol{\sigma}$, f is the yield function
4. *Obtain stress increments*:

$$\Delta\boldsymbol{\sigma}^{(k)}=-\mathbf{R}^{(k)}\mathbf{r}^{(k)}-\delta\lambda^{(k)}\mathbf{R}^{(k)}\mathbf{q}^{(k)}$$

5. *Update plastic strain*:

$$\boldsymbol{\varepsilon}^{\mathrm{p}(k+1)}=\boldsymbol{\varepsilon}^{\mathrm{p}(k)}+\Delta\boldsymbol{\varepsilon}^{\mathrm{p}(k)}=\boldsymbol{\varepsilon}^{\mathrm{p}(k)}-[\mathbf{D}^{\mathrm{e}}]^{-1}\Delta\boldsymbol{\sigma}^{(k)}$$

$$\Delta\lambda^{(k+1)}=\Delta\lambda^{(k)}+\delta\lambda^{(k)}$$

$$\boldsymbol{\sigma}^{(k+1)}=\boldsymbol{\sigma}^{(k)}+\Delta\boldsymbol{\sigma}^{(k)}$$

6. $k=k+1$, go to 2

DOI: 10.1002/nag

APPENDIX B: DERIVATIVES USED BY CPPM IN PRINCIPAL STRESS SPACE

Stress invariants:

$$I_1 = \sigma_1 + \sigma_2 + \sigma_3$$

$$I_2 = \sigma_1\sigma_2 + \sigma_2\sigma_3 + \sigma_1\sigma_3$$

$$I_3 = \sigma_1\sigma_2\sigma_3$$

Yield function:

$$f = K_{\mathrm{MN}}\frac{I_3}{I_2} - I_1$$

$$K_{\mathrm{MN}} = \frac{9 - \sin^2\phi'_c}{1 - \sin^2\phi'_c}$$

Plastic potential function:

$$g = K_{\mathrm{MNG}}\frac{I_3}{I_2} - I_1$$

$$K_{\mathrm{MNG}} = \frac{9 - \sin^2\psi}{1 - \sin^2\psi}$$

First-order derivatives:

$$\mathbf{f} = \left[\frac{\partial f}{\partial \sigma_1}, \frac{\partial f}{\partial \sigma_2}, \frac{\partial f}{\partial \sigma_3}\right]$$

$$\frac{\partial f}{\partial \sigma_1} = K_{\mathrm{MN}}\left(\frac{\sigma_2\sigma_3}{I_2}\right)^2 - 1$$

$$\frac{\partial f}{\partial \sigma_2} = K_{\mathrm{MN}}\left(\frac{\sigma_1\sigma_3}{I_2}\right)^2 - 1$$

$$\frac{\partial f}{\partial \sigma_3} = K_{\mathrm{MN}}\left(\frac{\sigma_1\sigma_2}{I_2}\right)^2 - 1$$

$$\mathbf{q} = \left[\frac{\partial g}{\partial \sigma_1}, \frac{\partial g}{\partial \sigma_2}, \frac{\partial g}{\partial \sigma_3}\right]$$

$\partial g/\partial\sigma_1, \partial g/\partial\sigma_2$ and $\partial g/\partial\sigma_3$ are similar to $\partial f/\partial\sigma_1, \partial f/\partial\sigma_2$ and $\partial f/\partial\sigma_3$

Second-order derivatives:

$$\frac{\partial^2 g}{\partial \sigma_1^2} = -2K_{\mathrm{MNG}}\left(\frac{\sigma_2\sigma_3}{I_2}\right)^2\left(\frac{\sigma_2 + \sigma_3}{I_2}\right)$$

DOI: 10.1002/nag

$$\frac{\partial^2 g}{\partial \sigma_2^2} = -2K_{\mathrm{MNG}} \left(\frac{\sigma_1 \sigma_3}{I_2}\right)^2 \left(\frac{\sigma_1 + \sigma_3}{I_2}\right)$$

$$\frac{\partial^2 g}{\partial \sigma_3^2} = -2K_{\mathrm{MNG}} \left(\frac{\sigma_1 \sigma_2}{I_2}\right)^2 \left(\frac{\sigma_1 + \sigma_2}{I_2}\right)$$

$$\frac{\partial^2 g}{\partial \sigma_1 \partial \sigma_2} = \frac{\partial^2 g}{\partial \sigma_2 \partial \sigma_1} = 2K_{\mathrm{MNG}} \frac{\sigma_1 \sigma_2 \sigma_3^3}{I_2^3}$$

$$\frac{\partial^2 g}{\partial \sigma_1 \partial \sigma_3} = \frac{\partial^2 g}{\partial \sigma_3 \partial \sigma_1} = 2K_{\mathrm{MNG}} \frac{\sigma_1 \sigma_3 \sigma_2^3}{I_2^3}$$

$$\frac{\partial^2 g}{\partial \sigma_2 \partial \sigma_3} = \frac{\partial^2 g}{\partial \sigma_3 \partial \sigma_2} = 2K_{\mathrm{MNG}} \frac{\sigma_2 \sigma_3 \sigma_1^3}{I_2^3}$$

APPENDIX C: CONSISTENT ELASTOPLASTIC MODULUS

Spectral decomposition:

$$\boldsymbol{\sigma} = \sum_{i=1}^{3} \sigma_i \mathbf{m}_i$$

where σ_i, $i = 1, 2, 3$ are principal stresses

$$\mathbf{m}_i = \frac{\partial \sigma_i}{\boldsymbol{\sigma}}$$

where

$$\mathbf{m}_i = \frac{\sigma_i}{d_i}\left[\boldsymbol{\sigma} + (\sigma_i - I_1)\mathbf{I} + \frac{I_3}{\sigma_i}\boldsymbol{\sigma}^{-1}\right] \quad \text{and} \quad d_i = \prod_{j \neq i}^{3} (\sigma_i - \sigma_j)$$

$$\mathbf{f}^* = \sum_{i=1}^{3} f_i^* \mathbf{m}_i$$

where $f_i^* = \partial f / \partial \sigma_i$

$$\mathbf{q}^* = \sum_{i=1}^{3} q_i^* \mathbf{m}_i$$

where $q_i^* = \partial g / \partial \sigma_i$

$$\frac{\partial \mathbf{m}_i}{\partial \boldsymbol{\sigma}} = \frac{\sigma_i}{d_i}[I - I_3 \sigma_i^{-1} I_{\boldsymbol{\sigma}-1}] + \frac{\sigma_i}{d_i} \sum_{j=1}^{3} (I_3 \sigma_i^{-1} - \sigma_j^2)\sigma_j^2 \mathbf{m}_j \otimes \mathbf{m}_j$$

where $I = \frac{1}{2}[\delta_{ik}\delta_{jl} + \delta_{il}\delta_{jk}]$, $I_{\boldsymbol{\sigma}-1} = \frac{1}{2}[\sigma_{ik}^{-1}\sigma_{jl}^{-1} + \sigma_{il}^{-1}\sigma_{jk}^{-1}]$

DOI: 10.1002/nag

Consistent elastoplastic modulus:

$$\mathbf{E}^{\text{epc}} = \left(\mathbf{E}^{ea} - \frac{1}{h_a} \mathbf{E}^{ea} : \mathbf{q}^* \otimes \mathbf{f}^* : \mathbf{E}^{ea} \right) : \mathbf{E}^R$$

where

$$h_a = \mathbf{q}^* : \mathbf{E}^{ea} : \mathbf{f}^*$$

$$\mathbf{E}^R = \mathbf{I} - \Delta\lambda \mathbf{B} : \mathbf{D}^{\text{e}}$$

$$\mathbf{E}^{ea} = [(\mathbf{D}^{\text{e}})^{-1} + \Delta\lambda \mathbf{A}]^{-1}$$

$$\mathbf{A} = \sum_{i=1}^{3} \sum_{j=1}^{3} \frac{\partial q_i^*}{\partial \sigma_j} \mathbf{m}_i \otimes \mathbf{m}_j$$

$$\mathbf{B} = \sum_{i=1}^{3} f_i^* \mathbf{M}_i$$

$$\mathbf{M}_i = \frac{\partial \mathbf{m}_i}{\partial \boldsymbol{\sigma}}$$

ACKNOWLEDGEMENTS

The authors wish to acknowledge the support of NSF grant CMS-0408150 on 'Advanced probabilistic analysis of stability problems in geotechnical engineering'.

REFERENCES

1. Matsuoka H, Nakai T. Stress-deformation and strength characteristics of soil under three different principal stresses. *Proceedings of JSCE* 1974; **232**:59–74.
2. Griffiths DV. Some theoretical observations on conical failure criteria in principal stress space. *International Journal of Solids and Structures* 1986; **22**(5):553–565.
3. Matsuoka H, Sun DA. Extension of spatially mobilized plane (SMP) to frictional and cohesive materials and its application to cemented sands. *Soils and Foundations* 1995; **35**(4):63–72.
4. Sun DA, Matsuoka H. An elastoplastic model for frictional and cohesive materials and its application to cemented sands. *Mechanics of Cohesive-Frictional Materials* 1999; **4**:525–543.
5. Matsuoka H, Sun DA. *The SMP Concept-based 3D Constitutive Models for Geomaterials*. Taylor & Francis: London, 2006.
6. Griffiths DV. Failure criteria interpretation based on Mohr–Coulomb friction. *Journal of Geotechnical Engineering* 1990; **116**(6):986–999.
7. Borja RI, Sama KM, Sanz PF. On the numerical integration of three-invariant elastoplastic constitutive models. *Computer Methods in Applied Mechanics and Engineering* 2003; **192**(9–10):1227–1258.
8. Simo JC, Taylor RL. Consistent tangent operators for rate-independent elastoplasticity. *Computer Methods in Applied Mechanics and Engineering* 1985; **48**(3):101–118.
9. Simo JC, Hughes TJR. *Computational Inelasticity*. Springer: New York, 1998.
10. Smith IM, Griffiths DV. *Programming the Finite Element Method* (4th edn). Wiley: Chichester, New York, 2004.
11. Bishop AW. The strength of soils as engineering materials. 6th Rankine lecture. *Géotechnique* 1966; **16**(9):91–130.
12. Bićanić N, Pearce CJ. Computational aspects of a softening plasticity model for plain concrete. *Mechanics of Cohesive-Frictional Materials* 1996; **1**(1):75–94.

DOI: 10.1002/nag

13. Péréz-Foguet A, Rodríguez-Ferran A, Huerta A. Consistent tangent matrices for substepping schemes. *Computer Methods in Applied Mechanics and Engineering* 2001; **190**(35–36):4627–4647.
14. Larsson R, Runesson K. Implicit integration and consistent linearization for yield criteria of the Mohr–Coulomb type. *Mechanics of Cohesive-Frictional Materials* 1996; **1**(4):367–383.
15. Prandtl L. über die Eindringungsfestigkeit (Härte) plastischer Baustoffe und die Festigkeit von Schneiden. *Zeitschrift für angewandte Mathematik und Mechanik* 1921; **1**:15–20.

DOI: 10.1002/nag